# Supplemental for 'A Regional Subseasonal-to-Seasonal (S2S) Ocean-Atmosphere Forecast System for Peru and Ecuador'

Ivonne Montes[1,2], Berlin Segura[1], Fiorela Castillón[1], Roger Manay[1], Fernando Campos[3], Boris Dewitte[4,5,6], Katerina Goubanova[4,7], Veronique Garcon[8], Didier Gazen[9], Kobi Mosquera[1], Ken Takahashi[1]

[1] Instituto Geofísico del Perú (IGP), Lima, Peru
[2] Universidad Ingeniería y Tecnología (UTEC), Lima, Peru
[3] Centro de Investigación Científica y de Educación Superior de Ensenada (CICESE), Ensenada, B.C., Mexico
[4] Centro de Estudios Avanzados en Zonas Áridas (CEAZA), Coquimbo, Chile
[5] Departamento de Biología Marina, Facultad de Ciencias del Mar, Universidad Católica del Norte, Coquimbo, Chile
[6] CECI, Université de Toulouse III, CERFACS/CNRS, Toulouse, France
[7] Météo France, Toulouse, France
[8] CNRS - Institut de Physique du Globe de Paris, Paris, France.
[9] Laboratoire d'Aérologie, Université de Toulouse, CNRS, UPS, Toulouse, France

*Correspondence to*: Ivonne Montes (imontes@igp.gob.pe)

Table S.1. Regional precipitation model performance metrics for five regions*

| Regions | Obs | RMSE (mm mo$^{-1}$) | R | Model mean (mm yr$^{-1}$) | Obs mean (mm yr$^{-1}$) | pBias (%) |
|---|---|---|---|---|---|---|
| C1 | GPM | 53 | 0.90 | 880 | 579 | 52.1 |
| C1 | PISCO | 59.9 | 0.91 | 880 | 459 | 92 |
| C2 | GPM | 113 | 0.58 | 3506 | 2924 | 19.9 |
| C2 | PISCO | 137 | 0.6 | 3506 | 2376 | 48 |
| C3 | GPM | 115 | 0.83 | 1929 | 831 | 132 |
| C3 | PISCO | 89.5 | 0.86 | 1929 | 1089 | 77 |
| E1 | GPM | 81.2 | 0.90 | 1847 | 1411 | 30.9 |
| E1 | PISCO | 118 | 0.89 | 1847 | 868 | 113 |
| E2 | GPM | 133 | 0.50 | 2227 | 3410 | -34.7 |
| E2 | PISCO | 93.9 | 0.52 | 2227 | 2340 | -5 |
| O1 | GPM | 17.5 | 0.92 | 100 | 116 | −13.4 |
| O2 | GPM | 2.9 | −0.25 | 21.1 | 21.6 | -2.2 |

*Metrics include Root Mean Square Error (RMSE) and Pearson Correlation (R) of the monthly series, observed and simulated annual precipitation mean and the percent bias (pBias)

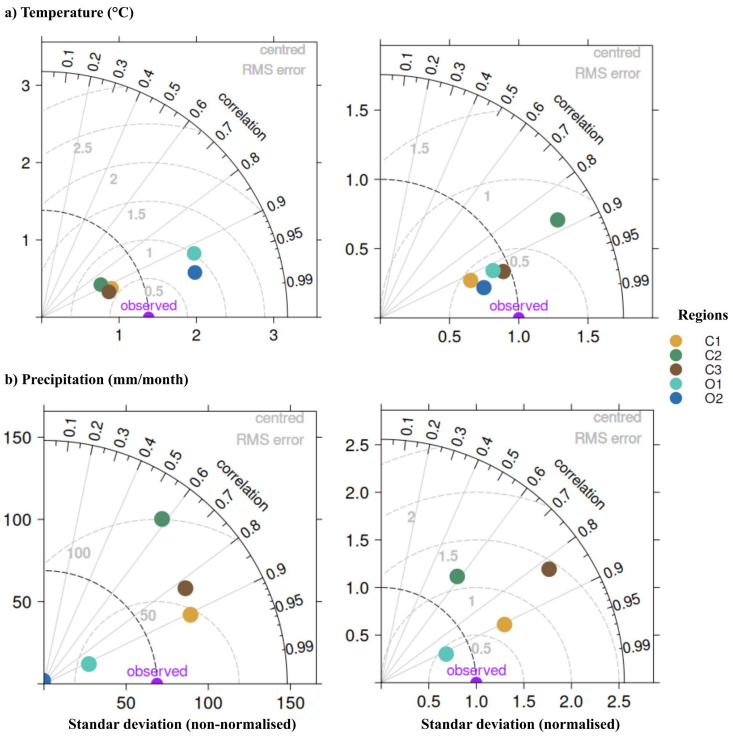



Figure S1. Taylor diagrams of monthly values for (a) 2-m air temperature and (b) sea surface temperature (SST), evaluated over five regions: (1) the northern oceanic region within El Niño 1+2 area (O1: 81.5°-84.5° W, 3.5°-6.5° S), (2) the coastal region off Lima (O2: 80°-78° W / 11°-13.5° S), (3) the northern coast (C1: 81°-79.3°W / 4°-6°S , (4) the Amazon region (C2: 75°-72° W, 3.5°-5.5° S) and (5) central Andes or Mantaro valley (C3: 76°-74° W / 11°-13.5° S). The left column shows the non-normalized diagrams, while the right column presents the normalized diagrams. Each point represents the regional model performance in terms of standard deviation, correlation coefficient, and centered root mean square error , relative to the observations (ERA5 and AVHRR products)

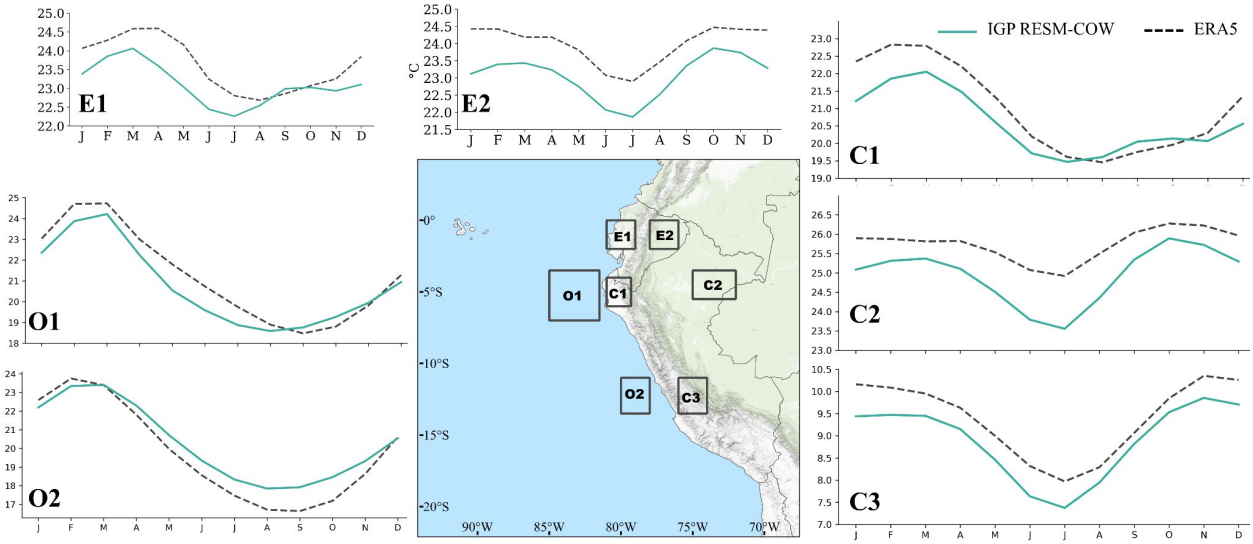



Figure S2. Annual cycle of 2m air temperature computed from the climatology of the coupled ocean-atmosphere model and the observations of ERA5 (grey bars) reanalysis product for 2001-2025 period across five regions: (1) the northern oceanic region within El Niño 1+2 area (O1: 81.5°-84.5° W, 3.5°-6.5° S), (2) the coastal region off Lima (O2: 80°-78° W / 11°-13.5° S), (3) the northern coast (C1: 81°-79.3°W / 4°-6°S , (4) the Amazon region (C2: 75°-72° W, 3.5°-5.5° S), (5) central Andes or Mantaro valley (C3: 76°-74° W / 11°-13.5° S), and two regions in Ecuador following Ilbay-Yupa et al. (2021): E1 (81° -79° W, 0-2 °S, corresponding to regions R2, R3 and R5 in their Figure 5, and E2 (78° -76° W, 0-2 °S), corresponding to regions R21 and R22.

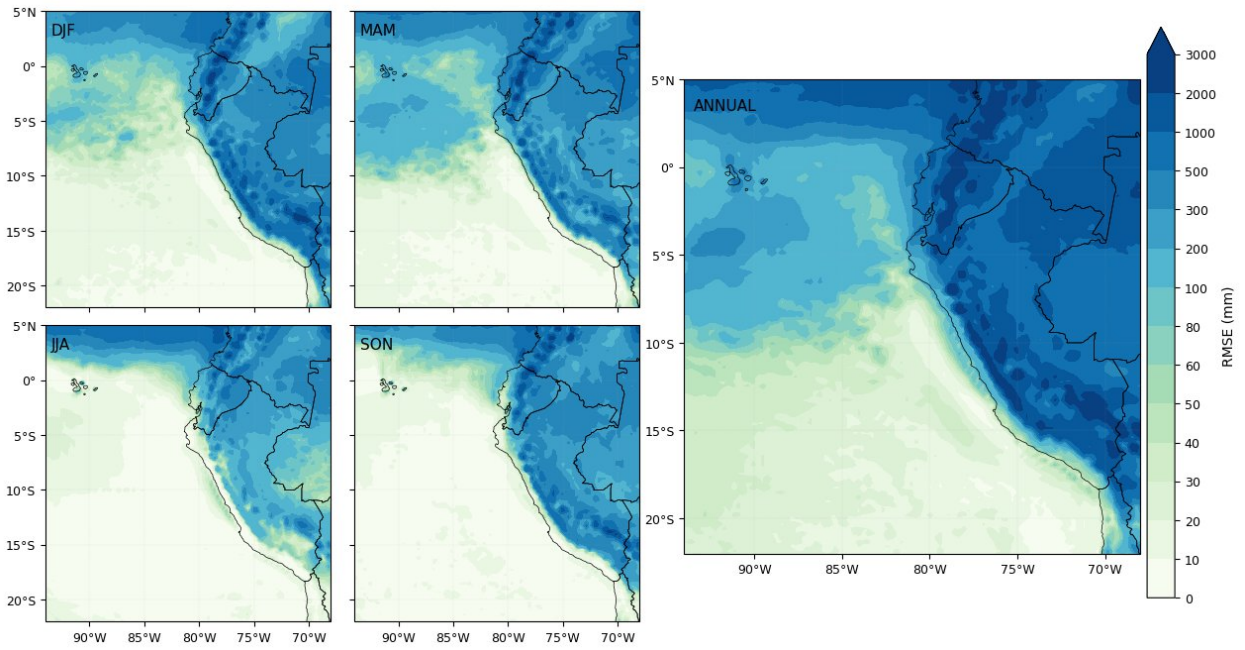



Figure S3. Spatial distribution of the root mean square error (RMSE) of accumulated precipitation for the seasonal periods DJF, MAM, JJA, and SON (left panels, mm season$^{-1}$), and for the annual accumulated precipitation (right panel, mm year$^{-1}$). RMSE is computed by comparing IGP RESM-COW simulated precipitation against observations (GPM product).

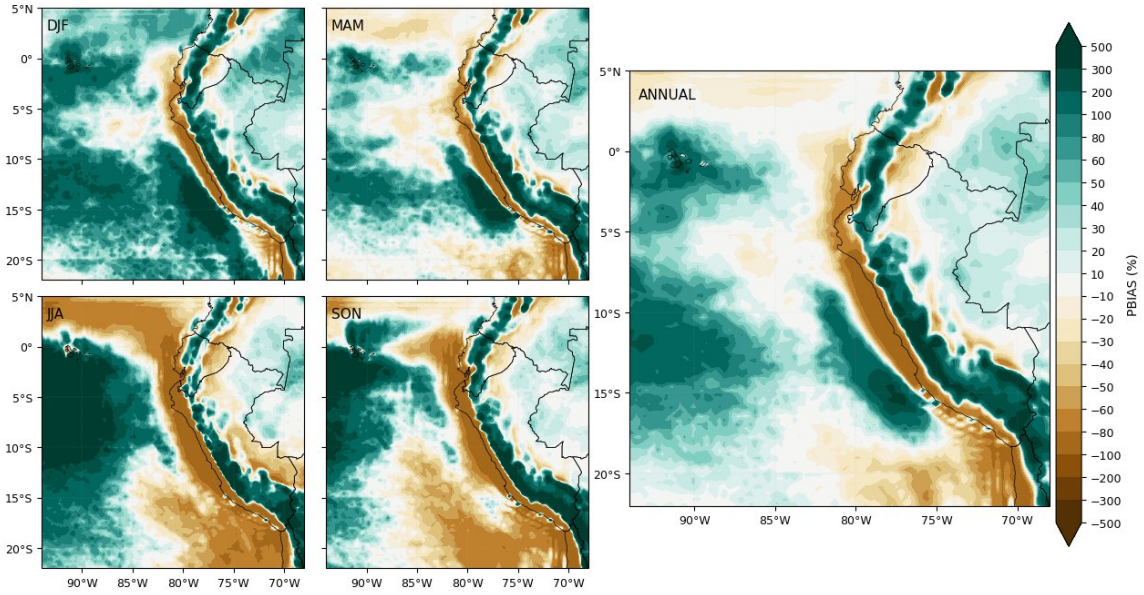



Figure S4. Spatial distribution of the percentage bias (pBIAS) of accumulated precipitation for the seasonal periods DJF, MAM, JJA, and SON (left panels), and for the annual accumulated precipitation (right panel). Green shades indicate positive pBIAS values corresponding to precipitation overestimation by the model, while brown shades indicate negative pBIAS values associated with underestimation by the model relative to observations (GPM product). Units are expressed as percentages (%)

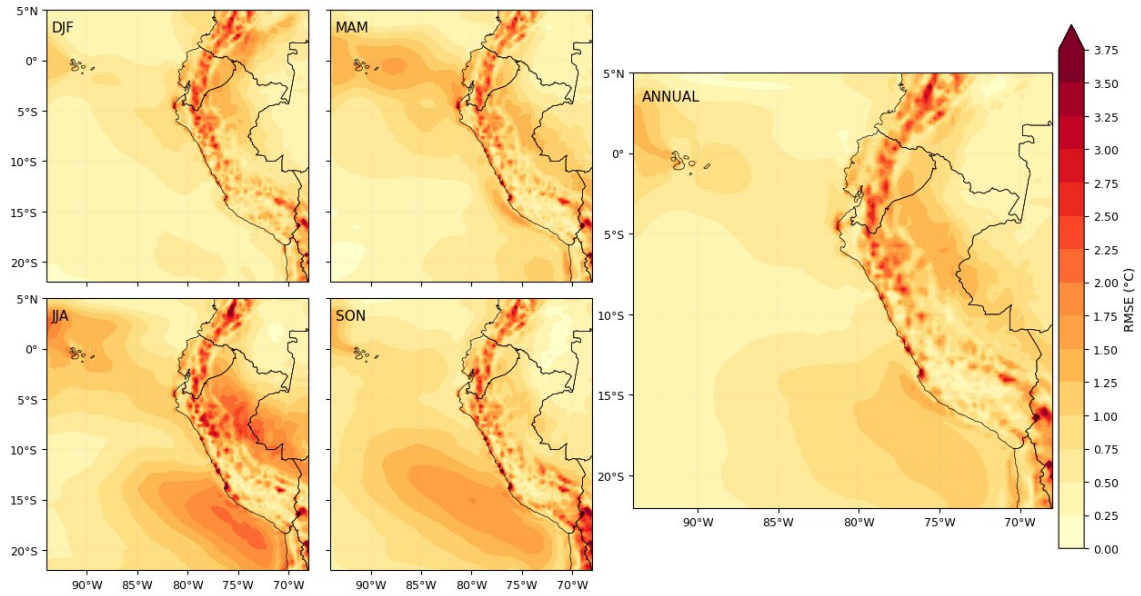



Figure S5. Spatial distribution of the root mean square error (RMSE) of 2m air temperature mean for the seasonal periods DJF, MAM, JJA, and SON (left panels, °C), and for the annual mean temperature (right panel, °C). RMSE is computed by comparing IGP RESM-COW simulated 2m air temperature against observations (ERA5 product).

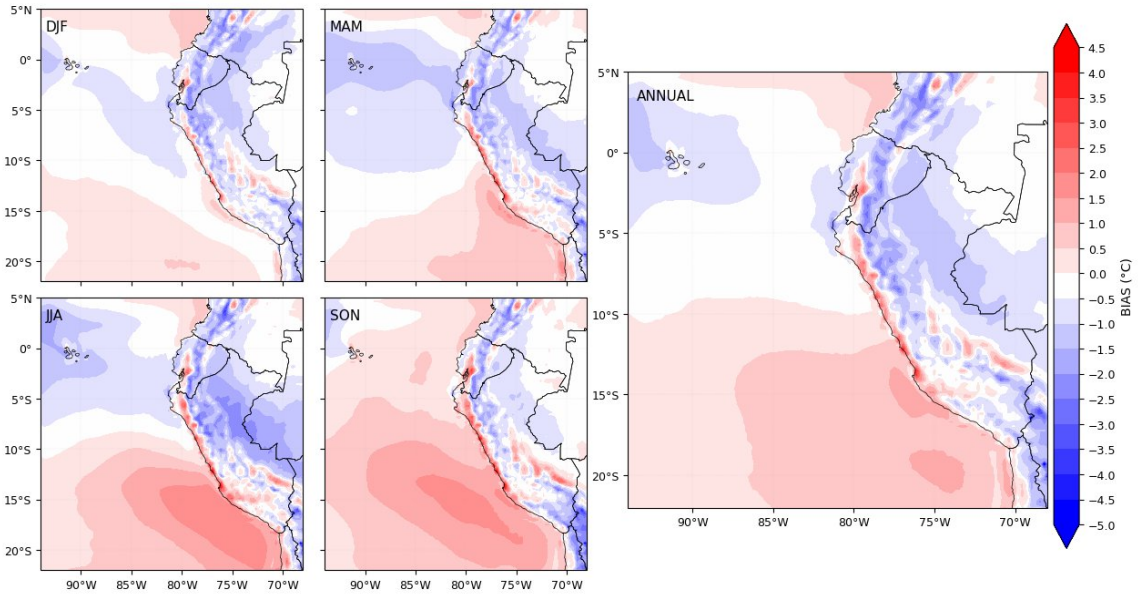



Figure S6. Spatial distribution of the bias in 2-m air temperature relative to ERA5 for the seasonal periods DJF, MAM, JJA, and SON (left panels), and for the annual mean (right panel). Red shades indicate positive bias values, corresponding to model overestimation, while blue shades indicate negative bias values, associated with underestimation of air temperature relative to ERA5. Units are expressed in degrees Celsius (°C).

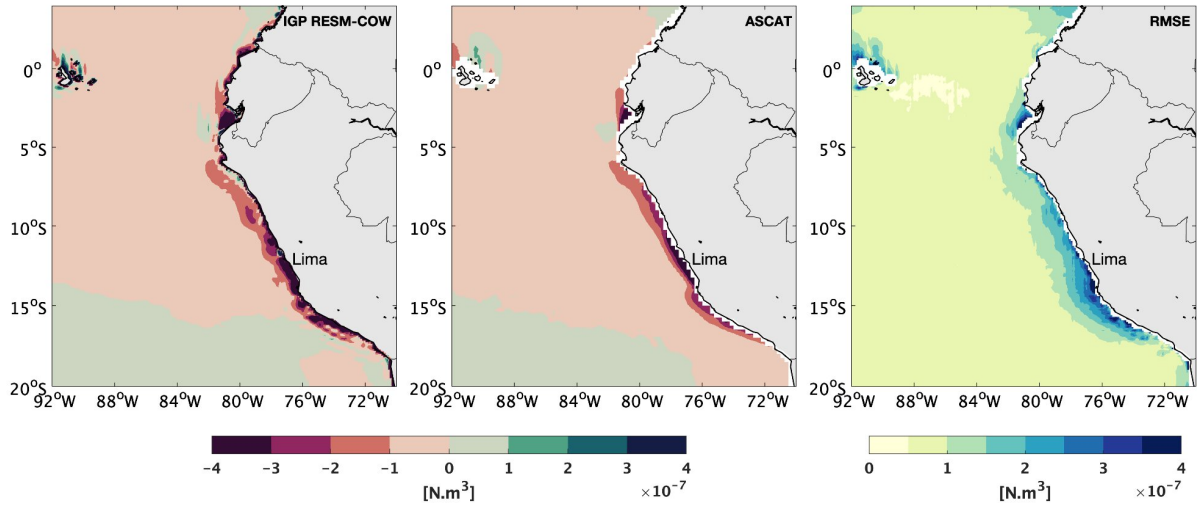



Figure S7. Spatial distribution of the annual mean wind stress curl over the 2001-2025 period for the entire domain from the IGP RESM-COW model (left), the ASCAT product (central), and the Root Mean Square Error (RMSE) between observations and model results (right).

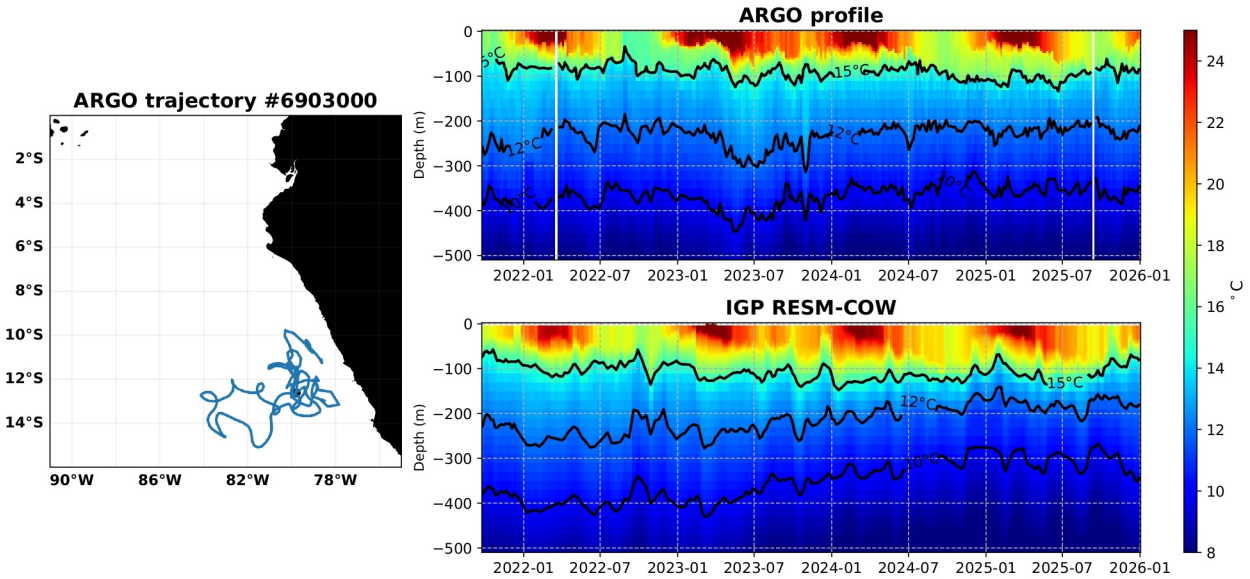



Figure S8. Trajectory of ARGO float 6903000 (left) and evolution of the upper ocean temperature (top 500 m) along the float path from ARGO observations (Top right) and the IGP RESM-COW simulation (Bottom right) from September 2021 and December 2025. Isotherms of 10°C, 12°C and 15°C are shown as black contour lines.

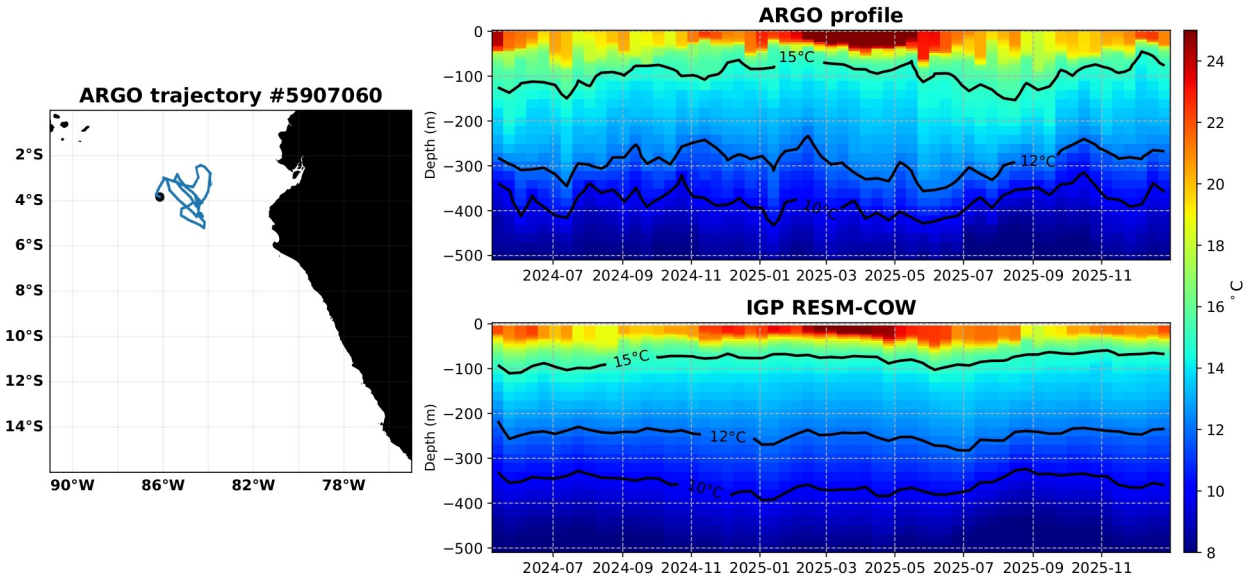



Figure S9. Trajectory of ARGO float 5907060 (left) and evolution of the upper ocean temperature (top 500 m) along the float path from ARGO observations (Top right) and the IGP RESM-COW simulation (Bottom right) from September 2021 and November 2025. Isotherms of 10°C, 12°C and 15°C are shown as black contour lines.

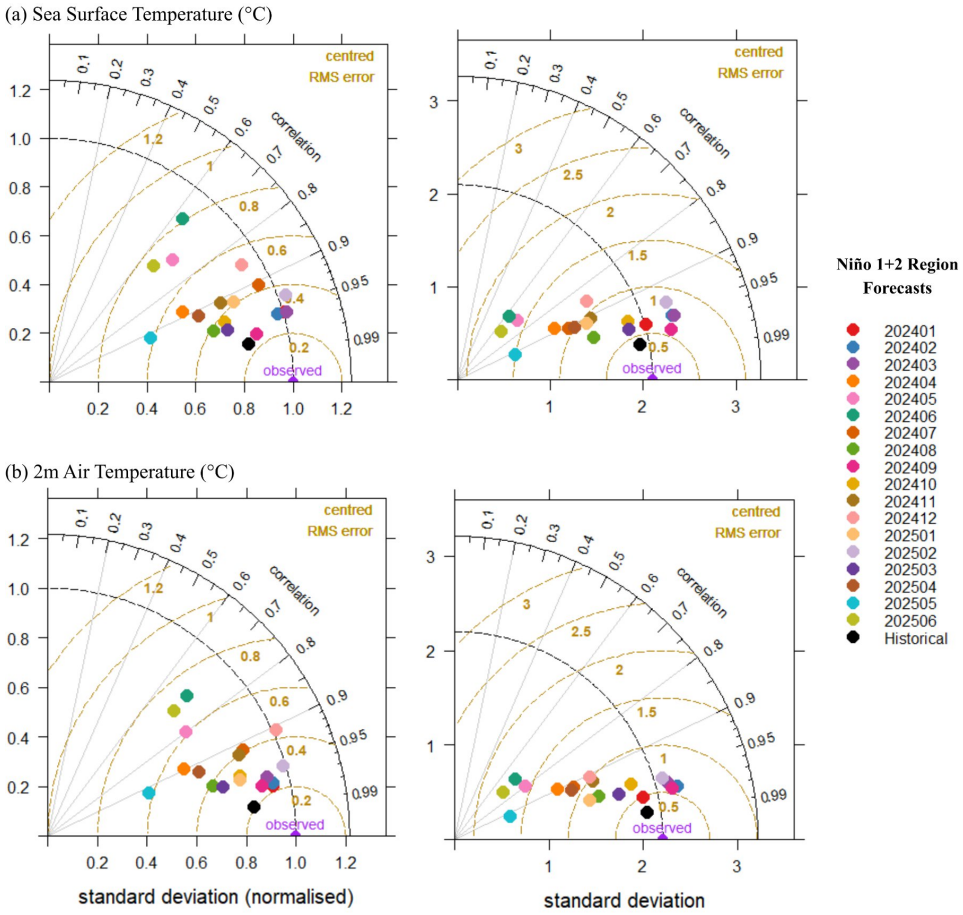



Figure S10. Taylor diagrams for (a) sea surface temperature (SST) and (b) 2-m air temperature, showing the performance of multiple forecast initializations over the Niño 1+2 region. The black marker represents the long-term coupled simulation (2000-2025), while colored markers correspond to individual forecasts. The left column displays the normalized Taylor diagrams, and the right column shows the non-normalized diagrams. Model performance is evaluated in terms of standard deviation, correlation coefficient, and centered root mean square error, relative to the observations (AVHRR and ERA5).

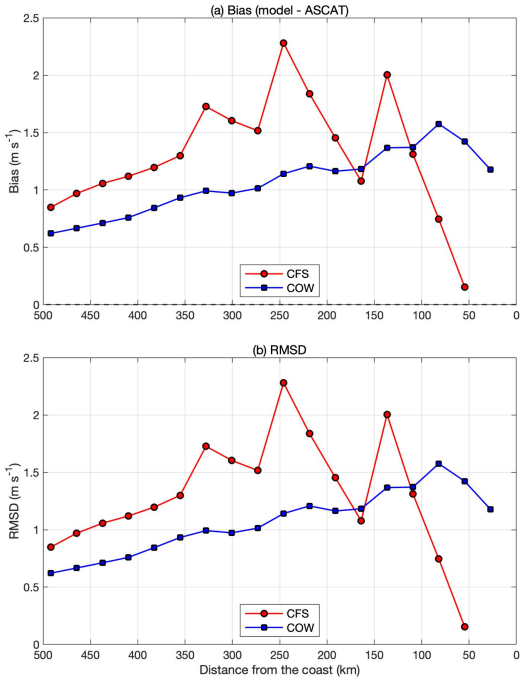



Figure S11. Bias (upper panel) and RMSD (lower panel) of the climatological alongshore wind speed for CFS (red circles) and IGP RESM-COW (blue squares) relative to ASCAT, as a function of offshore distance up to 500 km. Bias is defined as model − ASCAT; positive values indicate stronger winds in the models. Missing values near the coast reflect the absence of valid ocean points in the respective model grids.

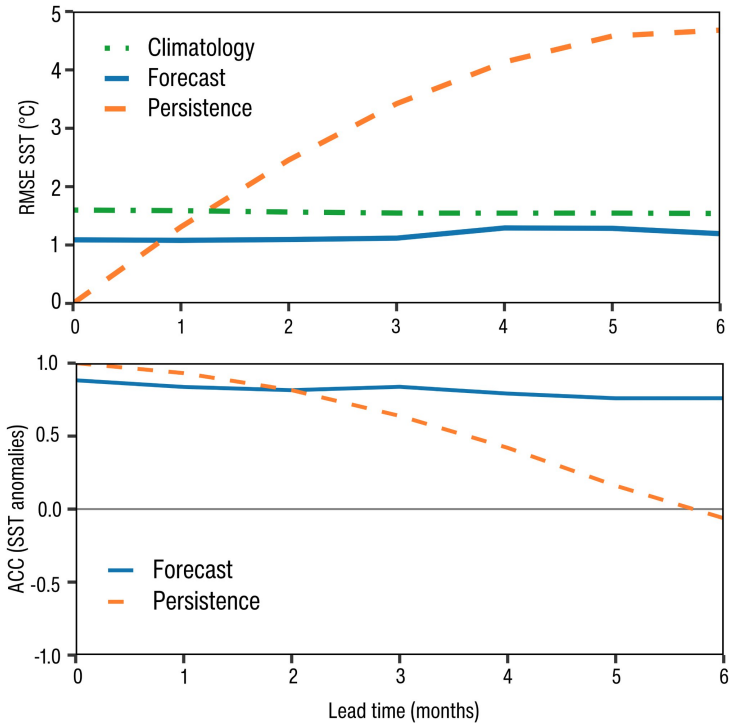



Figure S12. RMSE of monthly mean SST (Top) and anomaly correlation coefficient (ACC) of monthly SST anomalies (Bottom) in the Niño 1+2 region as a function of lead time. Forecast skill from the IGP RESM-COW coupled model is evaluated using 34 independent forecasts initialized between September 2022 and June 2025, each integrated for up to seven months (blue solid line). Monthly SST anomalies are defined relative to a 2001-2025 monthly climatology, without detrending. Forecast performance is compared against persistence (orange dashed line) and observed monthly climatological reference (green dashed line). RMSE values are expressed in °C, while ACC indicates the linear correlation between forecasted and observed SST anomalies.